FUDMA Journal of Sciences (FJS)
ISSN online: 2616-1370
ISSN print: 2645 - 2944
Vol. 10 No. 8, April, 2026, pp 28 – 39
DOI: https://doi.org/10.33003/fjs-2026-1007-5264

INTEGRATED GEOELECTRICAL AND PUMPING-TEST ASSESSMENT OF AQUIFER CHARACTERISTICS IN METROPOLITAN KANO, NORTHWESTERN NIGERIA

***Sani Yakubu Khalifa and Mohammed Aliyu Aliyu**

Department of Water Resources and Environmental Engineering, Faculty of Engineering, Ahmadu Bello University Zaria, Kaduna State, Nigeria.

*Corresponding authors' email: Khalees2k1@gmail.com
(ORCID: 0000-0002-2036-4835)

ABSTRACT

Groundwater is the major source of water supply in arid and semi-arid regions around the world. However, the depletion of groundwater resources has become a serious issue in many places due to excessive extraction combined with climate change impacts. This study aims to evaluate the current state of groundwater depletion and its socioeconomic consequences in Kano metropolitan. The research combines data analysis of groundwater levels using previous pump test data, the integration of Geophysical investigation employing vertical electrical sounding (VES) and GIS approaches to an alyze the groundwater level using the widely accepted MODFLOW-2005 model. The results show that groundwater levels have declined steadily over the past few decades due to increasing water demand from the growing population, agricultural expansion, and industrial development. The resistivity method used in has greatly assisted in delineating subsurface. The interpreted results of the thirty-seven (37) points were showing three to five subsurface layers which include topsoil, lateral soil, weathered rock, fractured basement and fresh basement varied from 3.515 to 10297-ohm m, 10.99 to 1508.5-ohm m, 0.919 to 953.95-ohm m, 2.086 to 15190-ohm m and 0.0106 to 42304-ohm m respectively. Dar-Zarrouk parameters such as longitudinal conductance (S) and transverse resistance (R) values varied from 0.000426 to 6.168041 Ω^{-1} and 25.57056 to 125809.6 Ωm^2 respectively. GIS complements these methods by enabling the visualization and spatial analysis of groundwater-related data. Through the integration of aquifer characteristic and geophysical data. The findings emphasize that over-extraction for urbanization, and industrial use, combined with insufficient natural recharge and changes in land use, are significant drivers of groundwater depletion. Incorporating previous pump test data analysis by providing detailed information on aquifer properties such as transmissivity, hydraulic conductivity, specific yield and storativity with a ranging value between 0.157– 4.285m²/d, 0.0225 to 0.4569 m/d, 0.0162, 0.05 0.0696 m3/min and 0.056 and 0.579 respectively.

Keywords: Groundwater, Depletion, Resistivity, Pump, Aquifer

INTRODUCTION

Groundwater is the water found underground in the cracks and spaces in soil, sand, and rock. It is stored and moves slowly through geological formations of soil called aquifers. Baba & Tyfur (2011) traces the term aquifer_ as its latin origin; aqui mean aqua (water) and fer from ferre (to bear). All groundwater abstractions initially lead to a decrease of stored groundwater volume within the cone of depression of hydraulic heads around the pumping well. The cone of depression can stabilize if the lowered hydraulic heads have induced a decrease of base flow or an increase of groundwater recharge that balance the abstractions (Zhou et al, 2009 cited in Hannes et al, 2014). Then, groundwater storage stabilizes at a lower equilibrium level as compared to the situation without groundwater abstractions. If, however, groundwater abstractions cannot be balanced by increased recharge and decreased discharge over a number of years, a long-term decline of hydraulic heads and groundwater storage, i.e., groundwater depletion (GWD), will result.

Over exploitation of groundwater resources in urban Kano, increase in demand caused by rapid population growth and urbanization is of great concern. Haphazard and indiscriminate over lifting and over deletion of ground water within the city led to the rapid falling of groundwater level, thereby increasing the draw down with very little or zero seasonal recharge thereby drastically reducing the recovery rate.

Aquifer

An aquifer is a body of permeable rock or sediment that stores and transmits groundwater. Aquifers are vital for supplying fresh water to ecosystems, agriculture, and human populations. They are typically found underground and vary in size, depth, and capacity depending on the geological formations in which they occur. The ability of an aquifer to hold and move water depends on the porosity (the amount of open space between particles) and permeability (how easily water can flow through the material) of the rock or sediment (Abdulhamid, 2014).

Permeability

The ease with which water can move through earth materials is a function of the permeability of the materials on the other hand it's the capacity of rock and soil to allow water or other fluid such as soil to pass through, it depends more on the size of pore opening than on the percentage of pore space (Baishali Niyogi, 2023).

Groundwater Potential

Refers to the capacity of an area's subsurface to store and provide groundwater in usable quantities. Areas or zones of abundant groundwater available for use are referred to as areas of good groundwater potential. It is a critical factor for water resource management, especially in regions where surface water may be scarce or unreliable.

Causes of Ground Water Depletion

Groundwater depletion most commonly occurs because of the frequent pumping of water from the ground. We pump the water more quickly than it can renew itself, leading to a dangerous shortage in the groundwater supply. As a growing world with a population that continues to rise, the more we pump water from the ground at a rapid rate, the more difficult it is for the groundwater to provide us with the amount of water that we need (Galloway & Cunningham, 2003; Rinkesh et al., 2018).

MATERIALS AND METHODS

Study Area

Kano metropolis is located in the Northwestern Nigeria on Latitude 11°55 to 12°07' N and Longitude 8°25'E to 8°40'E within the semi-arid Sudan savannah zone of West Africa. Kano has a mean height of about 481 m above sea level (Mustapha *et al*., 2014). The state was created on May 27, 1967 from part of the Northern region, Kano State borders Katsina State to the north-west, Jigawa State to the north-east, Bauchi State to the south-east and Kaduna State to the south-west.

Kano Metropolitan Area consists of eight Local Government Areas which include Fagge, Dala, Gwale, Kano Municipal, Tarauni, Nassarawa, Kumbotso and Ungogo LGAs with total area of 499 km^2 and a total population of 2,828,86l people (NPC, 2006). The latest official estimate (for 2023) is 4,348,000 inhabitants and it does suffice to say that the city is densely populated.

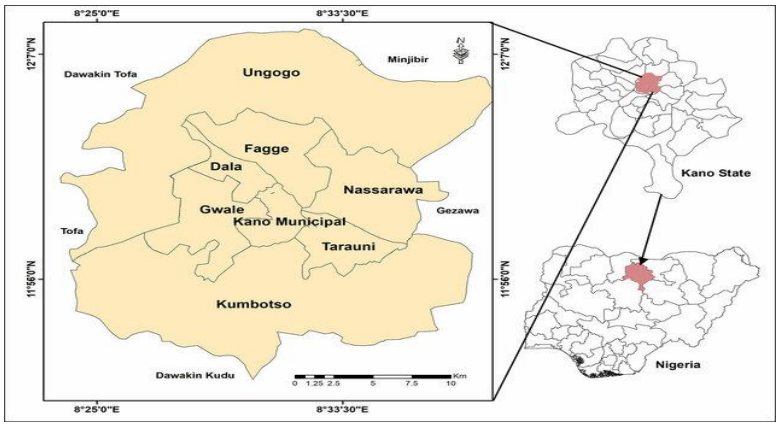

Figure 1: Study Area Map

Kano City is the second largest industrial center after Lagos State in Nigeria and the largest in the Northern Nigeria with textile, tanning, footwear, cosmetics, plastics, pharmaceuticals, ceramics, furniture, food and beverages and other industries (Mustapha *et al*., 2014).

Geology and Hydrogeology of the Study Area

Kano area is underlain by rocks of the Nigerian basement complex comprising migmatites-gneiss complex, younger metasediments, older and younger granites (Bala et al., 2011). MacDonald et al. (1986) established that, it is dominantly underlain by undifferentiated metamorphic suite, older granite, coarse pink granite and porphyritic biotite granite. The predominant rock type is older granite.

Climate

Kano metropolitan is located in the tropics, a region characterised by alternating wet and dry conditions, with annual mean rainfall of 800mm occurring between April/May and September/October with peak in July and August. Great temporal variation occurs in the amount of rainfall received and no two consecutive years record the same amount. The movement of the tropical maritime air masses from the southwest to the North determines the weather of Kano State during the wet season (Mustapha et al., 2014).

Population Land Use and Settlement

Large population concentrates in the Kano metropolitan Local Government areas. The Population of Kano metropolitan area in 2006 census is as follows Fagge 200,095 with Area of 21 km^2, Dala 418,759 with Area 19 km^2, Gwale 357,827 with Area of 18 km^2, Kano Municipal 371,243 with Area 17 km^2, Tarauni 221,844 with Area 28, Nassarawa 596,411 with Area 34 km^2, Kumbotso 294,391 with Area 158 km^2 and Ungogo 365,737 with Area 204 km^2. This indicates that population is growing rapidly in both rural and urban areas of Kano State. Both Kano city centre and major towns of Kano State are densely populated.

Electrical Resistivity Survey

The resistivity technique examines horizontal and vertical discontinuities in the electrical properties of the ground. It measures earth resistivity by passing an electrical current into the ground and measuring the resulting potentials created. This method involves the supply of direct current or low frequency alternating current into the ground through a pair of electrodes and the measurement of the resulting potential through another pair of electrodes (potential electrodes). Because the current is known and the potential can be measured an apparent resistivity can be calculated. The apparent resistivity of the subsurface material is a function of the magnitude of the current the recorded potential difference and the geometry of the electrode array used. The current electrodes spacing (AB) increases after each reading while the potential electrodes spacing (MN) increases only when deemed necessary and controlled by the relation $\frac{AB}{2} \geq \frac{5MN}{2}$ as required by the Schlumberger array.

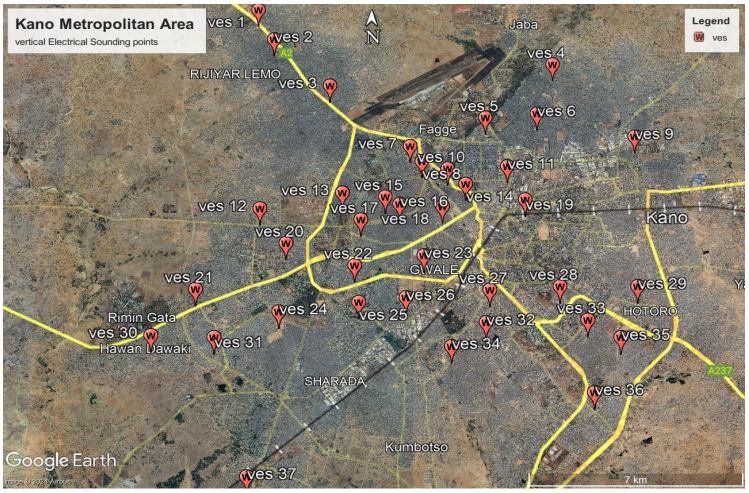

Figure 2: Study Area VES Points

The data was collected using Vertical Electrical Sounding (VES) in the selected areas as adopted from (Girish *et al*, 2009; Mosuro, 2012; Nwankwo, 2013). Earth resistance determinations were done using Alied Ohmega Terrameter. This is a portable microprocessor controlled integrated receiver and transmitter which provides a direct digital readout of resistance (Kollert, 1969).

Methods of Data Analysis

The Schlumberger method was adopted for this study because its fieldwork is faster, easier and more economical and softwares are readily available for its interpretation. The Schlumberger sounding techniques were carried out with current electrode spacing (AB) ranging from 2 to 200 m (AB/2 = 1 m to 100 m). The distances used for potential electrode spacing (MN) ranged from 0.4 m to 10 m (MN/2 = 0.2 m to 5 m). At each VES station, electrodes were placed in a straight line and the inter-electrode spreads were gradually increased about a fixed center. The potential electrodes were increased only when it became too small for reliable readings to be obtained and the separation did not exceed 5 m in any VES station.

Sounding data in the form of earth resistance measurements were converted to apparent resistivity values by multiplication with the geometric factor. The conversion was done using this formula

$R \propto DV/I$ *or* $R = K \times (DV/I)$ (1)

Where R is apparent resistivity (ohmmeter); DV = Voltage (potential drop) measured in milli-volt; I = current (milli-ampere); and K = Schlumberger constant of proportionality and was calculated Using the Formula:

$$K = \frac{\pi(\frac{AB}{2})^2 - (\frac{MN}{2})^2}{MN} \quad (2)$$

Where AB = Current electrode spacing and MN = spacing between potential electrodes of the Schulumberger. This formula was adopted from Grand and West.

The apparent resistivity depends on the injected current I, measured potential V, and the geometric factor K. Current injected into the subsurface is affected by many features of the strata such as priority organic components, minerals such as silt, clay, packing of void spaces, fluid presence, etc. in subsurface strata (Adekalu et al., 2022)

Thematic factors

Arcgis Softare

Groundwater recharge potentiality is closely linked to the physiography of the area (Zolekar 2018). The combined influence of these factors has identified the potential groundwater zones (Yeh et al. 2016). Most researchers have often used these parameters for groundwater assessment studies (Doke, 2018; Allafta et al., 2021; Kaewdum and Chotpantarat, 2021; Kumari and Singh 2021). In this study, eight thematic factors, i.e. slope (Slp), land use land cover (Lulc), soil texture (St), drainage density (Dd), vegetation (Vg), rainfall (Rf), lithology (Lt) and temperature (Temp) were chosen for groundwater depletion with the implementation of geophysical data and modflow software.

Determination of Aquifer Hydraulic Properties Using Pump Test Data

A pumping test data were collected from RUWASA to determine the hydraulic properties of the aquifer at each study site following standard procedure (e.g. Time-drawdown, distance-drawdown, and recovery data). All the data's contained coordinate, static water level, well depth and yield. Drawdown data were taken at specific intervals (i.e. 1, 2, 5, 10, 15, 25, 30, 60 min and then 2, 4, 6 hr) until steady state condition reached.

Jacob's Distance –Drawdown Method

Following the Cooper-Jacob distance–drawdown method, drawdowns were plotted along the vertical axis (arithmetic scale) and distance along the horizontal axis (logarithmic scale). The transmissivity (T, which measures the water transmitting capacity of the aquifer) and storage coefficient (S, which measures the aquifer's water storage ability) was determined following the procedure, as stated in Equation (3) and Equation (4)

$$T = \frac{2.303Q}{4\pi\Delta S} \quad (3)$$

$$S = \frac{2.25Tt}{r_0^2} \quad (4)$$

Where, T = Transmissibility, m3/day/m, Q = Pumping rate, m3/day, Δs = Drawdown per log cycle, m, t = Drawdown measuring time in hr., and, r_0= space from the test well to the intersecting point where the straight line meets the zero drawdown line, m

Jacob's Time-Drawdown Method

This method is appropriate only to the part in which equilibrium conditions are reached or a complete cone of depression has been developed. A time-drawdown graph was prepared on a semi-log paper with drawdown on the vertical axis (arithmetic scale) and time on the horizontal axis (logarithmic scale). Here, Jacob's correction was applied for

drawdown if $s^2/2H>0.003$ m for the water table aquifer (Winston 2009). The transmissivity (T) and storage coefficient (S) were determined following the procedure of (McDonald and Harbaugh 1988) as stated in Equation (5) and Equation (6)

$$T=\frac{2.303Q}{4\pi\Delta S} \quad (5)$$

$$S=\frac{2.25Tt_0}{r^2} \quad (6)$$

Where, T = Transmissibility, m^3/day/m, Q = Pumping rate, m^3/day, Δs = Drawdown per log cycle, m, t_o= Time taken at which the straight line crosses the zero drawdowns, hr., and r= distance of the observation well from the pumping well, m.

Modelling

Selection of the Model

In this study, using a graphical user interface (GUI) model MUSE, MODFLOW 2006 was used to analyse the groundwater flow. In the MODFLOW 2006, the hydraulic head of each cell was calculated by solving the groundwater flow equation; finite difference equation, and hydraulic stress (e.g. model boundaries, wells, precipitation, recharge, and evapotranspiration (McDonald and Harbaugh 1988). The Model MUSE graphical user interface (GUI) allows the users to bring all the input fles independently for analysis using the MODFLOW 2005 model that helps to modify the spatial and temporal boundary of the study (Winston 2009).

Governing Equation of Groundwater Flow Model

The 3D movements of groundwater through porous earth material usually described by the partial-differential equation (Eq.7):

$$\frac{\partial}{\partial x}\left(K_x h\frac{\partial h}{\partial x}\right)+\frac{\partial y}{\partial y}\left(K_y h\frac{\partial h}{\partial y}\right)+\frac{\partial y}{\partial z}\left(K_z h\frac{\partial h}{\partial z}\right)-W=S_C\frac{\partial h}{\partial t} \quad (7)$$

Here, *Kx*, *K*y and *K*z = hydraulic conductivity along the *x*, *y*, and *z* coordinate axes respectively, these are parallel to the major axes of hydraulic conductivity (*L*/*T*), h = potentiometric head (*L*);

W = volumetric flux per unit volume representing the source and/or sinks of water, with *W* < 0.0 for flow out of the groundwater system, and *W*>0.0 for flow into the system (T-1); Sc is the specific storage of the porous material (L-1), and *t* is time (T).

Finite Difference Equation

In the finite difference form, application of the continuity equation comprises of the summation of all input and output flows of the cell must be equal to the rate of change in storage within the cell. The continuity equation expresses with the balance of flow for a cell, with constant density groundwater can be represented as:

$$\sum Qi = SS\frac{\Delta h}{\Delta t}\Delta V \quad (8)$$

Qi= fow rate into the cell (*L*3/T); SS = specifc storage in the fnite-diference formulation, Δ*V* = volume of the cell (*L*3) and Δh = change in head over a time interval of length Δ*t*

Stress Packages

Grid Preparation and Layer Discretization

The groundwater model setup was done for the study area of approximately 571.06 km2 was discretized with a finite difference grid of cell size 400 m that was composed of 66 columns and 80 rows. In total, there is 5280 number of cells in the model whereas the number of active cells is 3997 and an inactive cell is 1283 (Fig. 3)

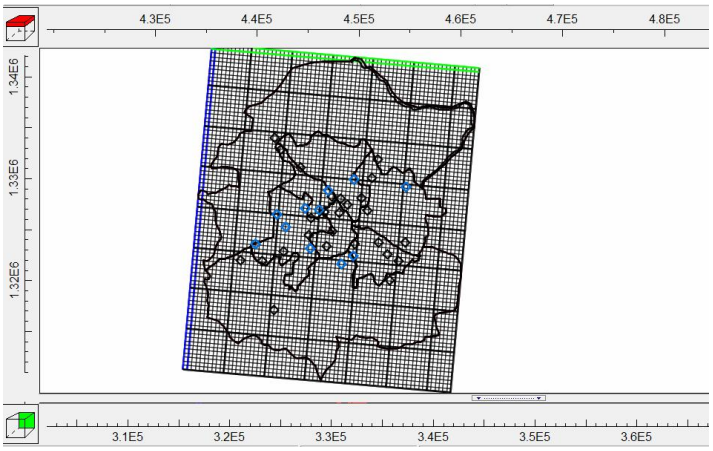

Figure 3: Conceptualization of the Study Area in Model MUSE

RESULTS AND DISCUSSION

Data collection

Firstly, A pumping test data of (2016) were collected from Kano Rural Water Supply and Sanitation Agency (RUWASA) and Kano state Ministry for local government which include there water level and aquifer yield, with their corresponding location and coordinates. Geophysical survey was conducted using vertical electrical sounding (VES) to know the groundwater potential zone with the aid of the pumping data coordinates,

VES Data and Field Curve Analysis

Thirty-seven (37) VES sounding data were analyzed with the IX1D software to delineate the subsurface layers as well as their depths, thickness and the resistivity values. Table 1 below shows the VES coordinate locations and elevations of the study area.

Fractured layer

The resistivity value ranges from 2.086 ohm m to 15190 ohm m. The thickness varies from 1.165 m to 54.32 m. (Dan Hassan et al., 2019) identified this layer to be the major aquifer unit. In some places, fractured zones occur immediately beneath the weathered horizon. Where the fractured zone is saturated, a high groundwater yield can be obtained from borehole penetrating such a sequence. If the depth of weathering is sufficiently thick as exhibited by most of the VES points in the study area; the weathered mantle could contain water in storage large enough to produce a successful borehole. Therefore, based on thickness and

resistivity of weathered layer; the following VES points are identified as good potentials for groundwater development; VES 1, 9, 11, 12, 13, 14, 15, 16, 17, 18, 20, 21, 22, 23, 24, 25, 26, 29, 31, and 34.

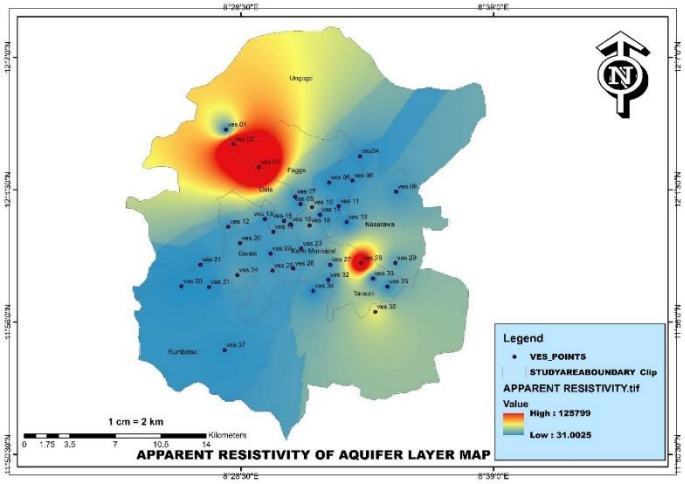

Figure 4: Spatial Distribution Map of Aquifer Apparent Resistivity over the Study Area

However, this layer (weathered) is believed to be the regolith. Invariably, they have a range of resistivity values. Hazell (1992) made it clear in their geophysical assessment of Kano crystalline aquifers that, the range reflects the preferred lithological range, high value indicates a granular regolith, and intermediates values indicating silty clayey regolith.

Table 1: Summary of Aquifer Characteristics and Dar Zarrouk Parameters Using the Geophysical Survey

VES No	Depth to aquifer (m)	Aquifer thickness h (m)	Apparent resistivity of aquifer ρa (Ωm)	Aquifer ConductiVity σ=1/ρ (ohm)	Transverse resistance R=hρ ($Ωm^2$)	Longitudinal conductance S = h/ρ ($Ω^{-1}$)	Hydraulic conductivity K (Ωm)	Transmissivity T = R ($Ωm^2$)
1	29.177	28.303	20.938	0.04776	592.6082	1.351753	20.938	592.6082
2	9.1377	5.2755	15190	6.58E-05	80134.85	0.000347	15190	80134.85
3	25.736	19.244	6537.6	0.000153	125809.6	0.002944	6537.6	125809.6
4	10.416	3.5747	120.3	0.008313	430.0364	0.029715	120.3	430.0364
5	8.5417	7.3611	23.003	0.043473	169.3274	0.320006	23.003	169.3274
6	14.304	13.687	75.174	0.013302	1028.907	0.182071	75.174	1028.907
7	7.415	5.4626	204.21	0.004897	1115.518	0.02675	204.21	1115.518
8	13.731	5.4149	106.32	0.009406	575.7122	0.05093	106.32	575.7122
9	22.832	19.407	97.262	0.010282	1887.564	0.199533	97.262	1887.564
10	5.9078	2.1233	4980.3	0.000201	10574.67	0.000426	4980.3	10574.67
11	21.073	16.41	55.094	0.018151	904.0925	0.297855	55.094	904.0925
12	42.739	35.494	49.89	0.020044	1770.796	0.711445	49.89	1770.796
13	17.84	17.115	63.703	0.015698	1090.277	0.268669	63.703	1090.277
14	25.4	18.343	5.7419	0.174158	105.3237	3.194587	5.7419	105.3237
15	18.095	16.738	158.72	0.0063	2656.655	0.105456	158.72	2656.655
16	47.809	47.173	85.432	0.011705	4030.084	0.55217	85.432	4030.084
17	28.451	24.528	99.108	0.01009	2430.921	0.247488	99.108	2430.921
18	33.325	31.05	219.02	0.004566	6800.571	0.141768	219.02	6800.571
19	4.0294	3.6147	17.352	0.05763	62.72227	0.208316	17.352	62.72227
20	62.07	54.32	53.185	0.018802	2889.009	1.021341	53.185	2889.009
21	30.39	14.789	26.664	0.037504	394.3339	0.554643	26.664	394.3339
22	28.355	21.98	40.475	0.024707	889.6405	0.543051	40.475	889.6405
23	25.391	23.624	88.631	0.011283	2093.819	0.266543	88.631	2093.819
24	40.24	39.797	112.15	0.008917	4463.234	0.354855	112.15	4463.234
25	45.026	40.595	72.863	0.013724	2957.873	0.557141	72.863	2957.873
26	41.695	37.252	75.545	0.013237	2814.202	0.49311	75.545	2814.202
27	7.1153	5.4851	517.45	0.001933	2838.265	0.0106	517.45	2838.265
28	50.654	45.443	1670.7	0.000599	75921.62	0.0272	1670.7	75921.62
29	55.83	49.709	83.567	0.011966	4154.032	0.59484	83.567	4154.032
30	10.036	4.9734	14.337	0.06975	71.30364	0.346893	14.337	71.30364
31	19.904	12.869	2.0864	0.479294	26.84988	6.168041	2.0864	26.84988
32	13.54	9.6331	57.257	0.017465	551.5624	0.168243	57.257	551.5624
33	9.9441	7.7793	3.287	0.304229	25.57056	2.366687	3.287	25.57056
34	21.101	15.702	6.9885	0.143092	109.7334	2.246834	6.9885	109.7334

VES No	Depth to aquifer (m)	Aquifer thickness h (m)	Apparent resistivity of aquifer ρa (Ωm)	Aquifer ConductiVity σ=1/ρ (ohm)	Transverse resistance R=hρ ($Ωm^2$)	Longitudinal conductance S = h/ρ ($Ω^{-1}$)	Hydraulic conductivity K (Ωm)	Transmissivity T = R ($Ωm^2$)
35	1.6543	1.6543	260.89	0.003833	431.5903	0.006341	260.89	431.5903
36	50.607	28.428	765	0.001307	21747.42	0.037161	765	21747.42
37	7.9216	3.951	163.29	0.006124	645.1588	0.024196	163.29	645.1588
Max						6.168041	15190	125809.6
Min						0.000426	2.0864	25.57056
Average						0.639998	868.204	9870.147

A spatial distribution map of transverse resistance generated (Fig. 5) shows a Dark and Light Blue very high area (southwards) and Green to Yellow indicates low areas on the map. The values obtained from the Dar Zarrouk parameters ranges from 25.57056 to 125809.6 $Ωm^2$ with an average value of 9870.147 $Ωm^2$. It is shown in (table. 1) that high T values were encompassing VES stations 3, 4, 5, 7, 8, 9, 13, 14, 15 and 16 in the study area, indicating fresh zone. The south-eastern and southern parts of the study area was characterized by low T.

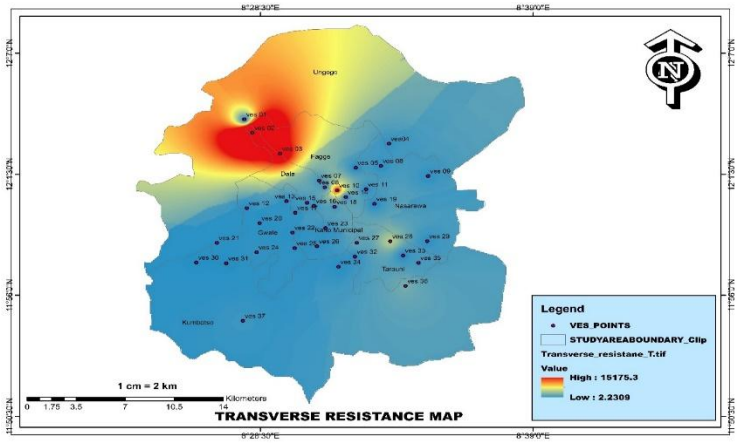

Figure 5: Spatial Distribution Map of Transverse Resistance over the Study Area

The Dar-Zarrouk (D-Z) parameters are highly useful to comprehend the spatial distribution of groundwater in addition to the geometry of the sub-surface units and provide an indication to aquifer prospective zones in the study area. The advantage of using D-Z parameters to estimate protective capacity is that the non-uniqueness of interpreting resistivity data is minimized. These parameters provide positive solutions as they reflect very clear, conspicuous and widely varying ranges of sub-surface resistivities. They also do not possess an overlapping character and in turn facilitate easy resolution. These results also give a useful first approximation of the D-Z parameter variations and could be used to site exploratory boreholes. The aquiferous zones are clearly reflected in the longitudinal conductance (S) and transmissivity (T) maps.

Land Use Land Cover

Land use land cover distribution map within the area was obtained for 2016 and 2024 as shown in Figure 6. From the analysis, it was realized that built -up areas increased gradually from 2016 to 2024. In 2016, built up areas covered an area of approx. 243.518 km^2 to 305.724 km^2 in 2024. This effect was attributed to the increase of population in the area that led to the development of towns and growth of settlements. Contrary to built-up areas, rangeland areas reduced from 256.418 km^2 in 2016 to 196.05 km^2 in 2024. The reduction was assigned to deforestation to create more land for settlement.

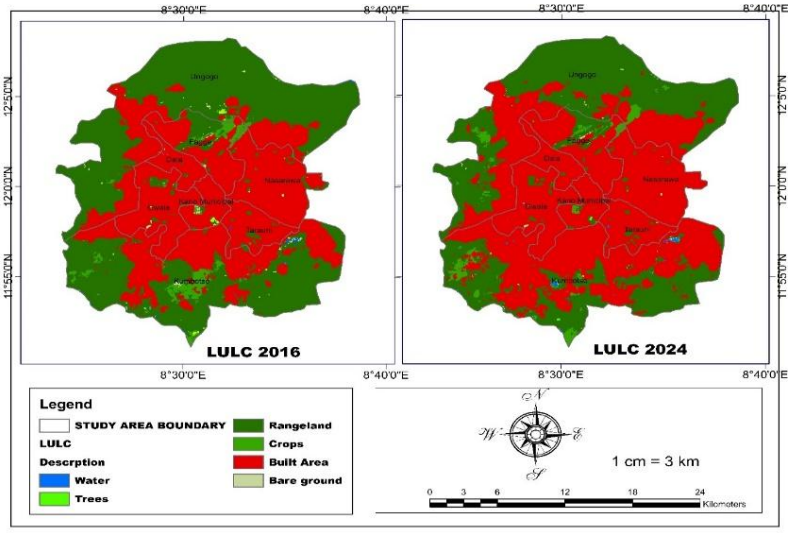

,

Figure 6: Land Use Land Cover Maps of the Study Area

Table 2: Summary and comparison between 2016 and 2024 land use land cover maps

S/N	Map Description	Lulc 2016		Lulc 2024	
		Area (km^2)	Percentage (%)	Area (km^2)	Percentage (%)
1	Water	0.815	0.158	1.056	0.205
2	Trees	0.810	0.157	0.198	0.038
3	Crops	12.246	2.376	10.599	2.057
4	Built area	243.518	47.25	305.724	59.320
5	Bare ground	1.575	0.306	0.810	0.175
6	Rangeland	256.418	49.753	196.05	38.206
TOTAL		515.382	100%	515.382	100%

Rainfall

CHIRPS data was processed to give the annual rainfall values for 2016, to 2024 in the study area as shown in Figure 6. The annual rainfall ranged from 517 mm to 621 mm in 2016, 656 mm to 684 mm in 2017, 466 mm to 525 mm in 2018, 588 mm to 655 mm in 2019, 622 mm to 673 mm in 2020, 479 mm to 561 mm in 2021, 521 mm to 609 mm in 2022 and 465 mm to 602 mm in 2023. The highland region of the county receives the highest rainfall through the study period.

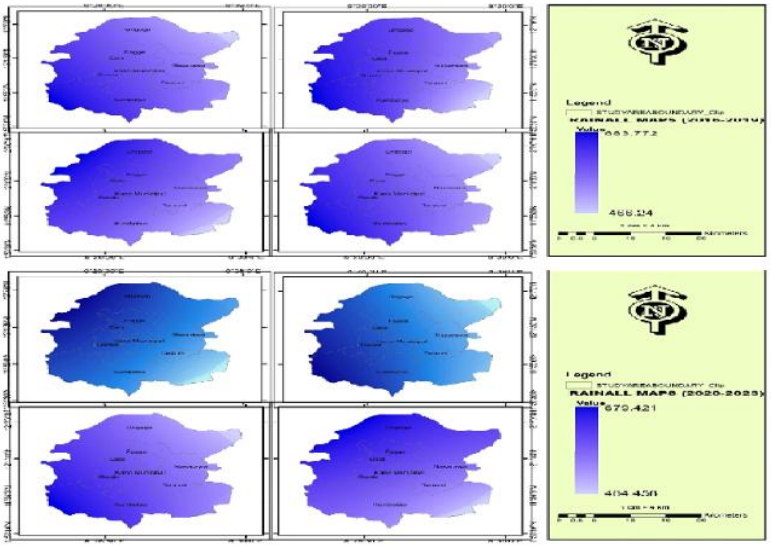

Figure 7: Rainfall Maps of the Study Area

Aquifer Properties Using Application of Cooper-Jacob method

The research was undertaken using (2016) pump test data to calculate the aquifer properties in the study area catchment using Aquifer_Test_Pro and AQTESOLV software by the application of Cooper-Jacob method. For this study pumping test data were collected in 37 operational wells in the research area.

Table 3: The Calculation of Well Data

Well No	Hydraulic Conductivity K (m/day)	Transmissivity (m^2/s)	Transmissivity (m^2/day)	Coefficient of Transmissivity (m^2/day)	class of Transmissivity magnitude	Storativity
1	0.1066	1.09×10^{-5}	1.045	1 to10	low	0.218
2	0.0313	7.26×10^{-6}	0.627	0.1 to 1	Very low	0.238
3	0.0851	4.84×10^{-6}	0.418	0.1 to 1	Very low	0.271
4	0.1073	1.75×10^{-5}	1.512	1 to10	Low	0.579
5	0.0609	1.33×10^{-5}	1.149	1 to10	Low	0.223
6	0.0534	1.91×10^{-5}	1.65	1 to10	Low	0.579
7	0.0541	2.06×10^{-5}	1.78	1 to10	Low	0.579
8	0.0507	2.01×10^{-5}	1.737	1 to10	Low	0.579
9	0.0479	9.30×10^{-6}	0.804	0.1 to 1	Very low	0.505
10	0.036	9.47×10^{-6}	0.818	0.1 to 1	Very low	0.204
11	0.0713	1.82×10^{-6}	0.157	0.1 to 1	Very low	0.474
12	0.0782	8.84×10^{-6}	0.764	0.1 to 1	Very low	0.056
13	0.1464	1.61×10^{-5}	1.391	1 to10	Low	0.101
14	0.1328	1.37×10^{-5}	1.192	1 to10	Low	0.260
15	0.0386	4.84×10^{-6}	0.942	0.1 to 1	Very low	0.228
16	0.4569	3.43×10^{-5}	2.964	1 to10	Low	0.579
17	0.1082	1.99×10^{-5}	1.719	1 to10	Low	0.579
18	0.0482	7.54×10^{-6}	0.651	0.1 to 1	Very low	0.217
19	0.0904	2.42×10^{-5}	2.091	1 to10	Low	0.468
20	0.0787	4.96×10^{-5}	4.285	1 to10	Low	0.579
21	0.0483	7.01×10^{-6}	0.606	0.1 to 1	Very low	0.086
22	0.0308	4.74×10^{-6}	0.41	0.1 to 1	Very low	0.146
23	0.0373	8.38×10^{-6}	0.724	0.1 to 1	Very low	0.500
24	0.1376	7.99×10^{-6}	0.69	0.1 to 1	Very low	0.251
25	0.0349	6.76×10^{-6}	0.584	0.1 to 1	Very low	0.335
26	0.153	1.99×10^{-5}	1.719	1 to10	Low	0.412
27	0.1121	1.45×10^{-5}	1.253	1 to10	Low	0.500
28	0.0225	1.22×10^{-5}	1.054	1 to10	Low	0.500
29	0.0268	1.75×10^{-5}	1.512	1 to10	Low	0.500
30	0.039	1.36×10^{-6}	0.864	0.1 to 1	Very low	0.500
31	0.0882	1.00×10^{-5}	1.175	1 to10	low	0.353
32	0.0316	5.19×10^{-6}	0.448	0.1 to 1	Very low	0.148
33	0.1079	7.26×10^{-6}	1.175	1 to10	low	0.183
34	0.1179	1.45×10^{-5}	1.253	1 to10	Low	0.500
35	0.0511	1.01×10^{-5}	0.873	0.1 to 1	Very low	0.410
36	0.0299	1.43×10^{-5}	1.236	1 to10	Low	0.500
37	0.0231	5.56×10^{-6}	0.48	0.1 to 1	Very low	0.184
MIN	0.0225	1.82×10^{-6}	0.157			0.056
MAX	0.4569	4.96×10^{-5}	4.285			0.579
AVERAGE	0.080405	1.299×10^{-5}	1.182486			0.365514

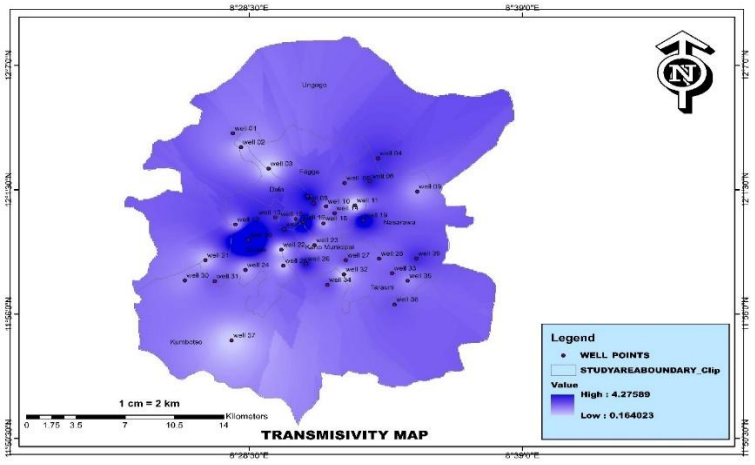

Figure 8: Spatial Distribution Map of Transmissivity over the Study Area

Modflow Model

Model Preparation

Groundwater table data of 2016 were obtained from RUWASA and Kano state Ministry for local government as the secondary data. The initial database were prepared for the geological and hydrogeological parameters based on the collected data. Along with these, hydraulic conductivity and specifc yield value of aquifer of the study area have been retained. Topographic maps and geological maps of this city were prepared by the downloaded grid data. Finally, with the help of ArcGIS 10.8, MODFLOW 2005 was prepared to simulate for the year 2016 to 2023.

Table 4: Summary of Study Area MODFLOW Model

S/N	Item	Details
1	Hydraulic conductivity	9.31×10–7 m/sec
2	Specific yield	0.0162 to 0.0696
3	Specific storage	0.056-0.579
4	Model simulation Type	Transient
5	Length of simulation	2016–2023 i.e. 8 years
6	Boundary package	CHD, RCH, WELL, EVT
7	Observations	Head observation

Model Calibration and Validation

Visual Modelmuse software was used for numerical modelling of the study area. However, in this study, the calibration results were obtained by comparing the predicted and observed head using PEST's Groundwater Utilities which are a set of MODLOW plugins. These operations were executed until the low error of calibration was obtained, thus, reflecting a reasonable calibration between simulated and observed heads and considerable representation of the real field. By MODFLOW analysis, using 2016 as a base year, water table data was generated for the years 2024. The result showed a significant difference between the observed and simulated hydraulic head of the year 2024 as shown in (figure 9).

Observation Name	Group Name	Object Name	Time	Measured	Modeled	Residual
Head_well_13	Not recorded	Observed_wells_13	8	17.3	22.967523572736	-5.667523572736
Head_well_21	Not recorded	Observed_wells_21	8	12.8	13.39141163019	-0.59141163019
Head_wells_12	Not recorded	Observed_wells_12	8	18.1	19.163082272733	-1.063082272733
Head_well_25	Not recorded	Observed_wells_25	8	13.1	16.921351005652	-3.821351005652
Head_well_20	Not recorded	Observed_wells_20	8	20.2	24.246917507381	-4.046917507381
Head_well_32	Not recorded	Observed_wells_32	8	13.9	14.462281547128	-0.562281547128
Head_well_15	Not recorded	Observed_wells_15	8	21.4	22.176413778421	-0.776413778421
Head_well_9	Not recorded	Observed_wells_9	8	11.8	11.478944464262	0.338944464262
Head_well_7	Not recorded	Observed_wells_7	8	10.2	13.687771845958	-3.487771845958
Head_well_34	Not recorded	Observed_wells_34	8	13.6	13.072528628407	0.532528628407
Head_well_5	Not recorded	Observed_wells_5	8	17.2	16.709761995096	0.259761995096

Figure 9: Comparison of Simulated Heads versus Observed Heads

A transient simulation for the same analysis period (2016–2024) was performed to analyse the head change over time. The analysis shows that, the adjustment of horizontal hydraulic conductivity (K_h), the value of the aquifer ensures the considerable match of the simulated and observed heads. According to the literature the average hydraulic conductivity value of the four aquifers was found 9.31×10^{-7} m/sec covering Top soil to the weathered layer). However, in the calibration period, the calibrated K_h value of the aquifer was 8.22×10^{-7} m/sec and also the available range of the specific storage value of 0.056 to 0.579 was adjusted to 0.037 from that ensured a reasonable match between the observed and simulated hydraulic head. To evaluate the calibration results, the mean absolute error (MAE), the root mean square error (RMSE), Percent Error (PE), and Mean Percent Error (MPE) were calculated from the following equations:

$$MAE = \frac{1}{n}\sum_{i=1}^{n}(O - S) \quad (7)$$

$$RMSE = \sqrt{\frac{\sum_{i=1}^{n}(O-S)^2}{n}} \quad (8)$$

$$PE = \frac{(O-S)}{S} \times 100 \quad (9)$$

$$MPE = \frac{100}{n}\sum_{i=1}^{n}\left(\frac{O-S}{S}\right) \quad (10)$$

Table 5: Calculation of the Percent Error (PE)

Well no	Observed	Simulated	Percent error (PE)
5	17.2	16.7	2.99
7	10.2	13.68	25.44
9	11.8	11.47	2.88
12	18.1	19.16	5.53
13	17.3	22.96	24.65
15	21.4	22.17	3.47
20	20.2	24.24	16.67
21	12.8	13.39	4.41
25	13.1	16.92	22.58
32	13.9	14.46	3.87
34	13.6	13.07	4.06

The observed MAE and RMSE were 1.816 and 2.664 successively. The percent error for the observed and simulated hydraulic head is given in (Table 5) above. The mean percent error for this final simulation was 10.6%. These outputs show that the simulation considerably measures the observed hydraulic head. At this time the model was validated for the year 2024 to justify the acceptability of all the calibrated values. Results showed a reasonable amount of validation with an R2 value of 0.766 (Figure. 10).

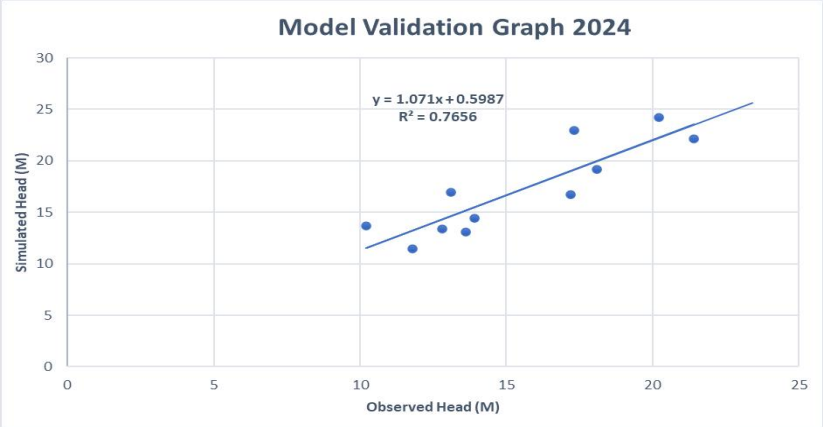

Figure 10: 2024 Model Validation Graph

Model Simulation

The hydraulic head distribution maps generated from the MODFLOW simulation over an eight-year period provide valuable insights into the spatial and temporal dynamics of groundwater within the Kano metropolitan area. These maps reflect how the aquifer system beneath the city responds to long-term stresses, particularly the effects of sustained groundwater abstraction and limited recharge in an urbanized environment.

The simulation of the model showed that kano city is experiencing an increasing trend of groundwater level depletion. Observation wells data showed that during the analysis period i.e. 2016–2024 North-western part of the area is facing the highest amount i.e. 12 m of groundwater level deletion with a ground water level of 39.64069m. Besides this, the south-east and central part of the study area are also facing an alarming rate of depletion.

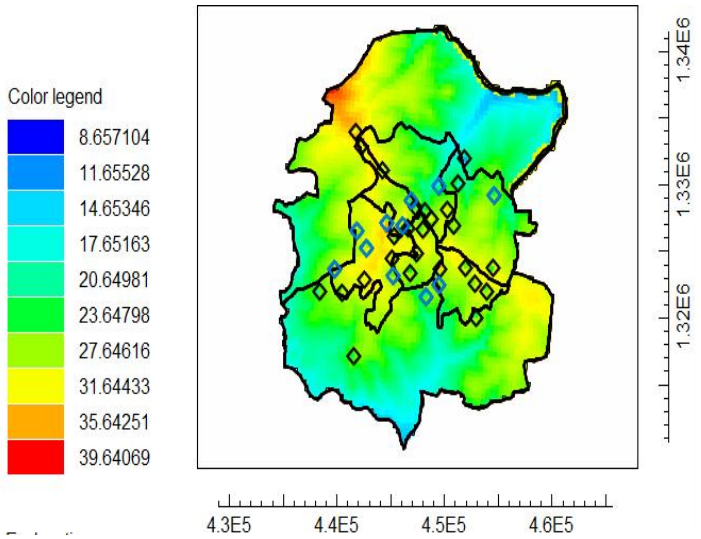

Figure 11: 2024 Hydraulic Head Distribution Map of the Study Area

This gradual reduction in head values, especially in zones of heavy pumping, highlights the growing pressure on the aquifer. The formation of drawdown cones around abstraction hotspots suggests that the rate of groundwater withdrawal has exceeded the rate of natural recharge, a common issue in highly urbanized and overpopulated areas with limited surface water supply. By year eight of the simulation, the maps clearly illustrated stressed areas with head values between 23.121–39.64 meters, compared to less affected zones with head values still in the range of 8.541–14.7855 meters as shown in (figure 11).

Each hydraulic head map is accompanied by a detailed legend that aids in interpretation. The legend typically displays a color gradient ranging from blue (lowest heads) to red (highest heads). In the case of this study, the color ramp used the following approximate values:

Dark Blue: (low head / high drawdown)
Light Blue – Green: (moderate head)
Yellow – Orange: (elevated head)
Red: (highest head / recharge zones)

The head distribution maps for Kano metropolitan area over the eight-year simulation period reveal a clear trend of declining groundwater levels, particularly in areas with high abstraction and limited recharge. The spatial and temporal patterns illustrated by the maps underscore the growing stress on the urban aquifer and highlight the need for improved water resource management strategies. The inclusion of detailed legends enhances the interpretability of the maps, making them effective tools for analysis and decision-making by water managers, planners, and local authorities.

CONCLUSION

Groundwater depletion in Kano city is due to the increased demand as a result of urbanization and if remedial measures fail to address this for both existing practices and future planning, possible sufferings could be the sinking of the city. The city experienced excessive groundwater extraction ended with land subsidence. In this study, to predict the groundwater lowering in Kano city, a numerical model study was done by a USGS code MODFLOW 2005. Assuming a constant recharge rate the model was run for 2016 to 2024. Comparison among 8 years during 2016–2024 showed the model simulated maximum depletion rate between 6.109-12m. Moreover, anthropogenic activities in this basin, such as excessive groundwater pumping for irrigation, industrial use, or municipal water supply, can significantly affect groundwater levels. Over-extraction of groundwater can lead to the lowering of water tables, causing a decline in groundwater levels. Additionally, land-use changes associated with agriculture and urbanization can impact the recharge of aquifers, reducing the replenishment of groundwater resources. Effective management and regulation of anthropogenic impacts on groundwater are essential to maintain sustainable groundwater levels and preserve the region's water resources.

REFERENCES

Abdulhamid, A. (2014): 'Drainage, Hydrology and Water Resources. In Kano: Environment, Society and Development, 1st ed.; Tanko, A.I., Momale, S.B., Eds.; Adonis and Abbey: London, UK; Abuja, Nigeria, 2014; Volume 1, pp. 21–34, ISBN 978190911291 (Paper Back), 9781909112407 (Hard Cover).

Adekalu, K., Osunbitan, J. Ojo, E., (2022): 'Water sources and demand in South Western Nigeria: implications for water development planners and scientists. Technovation, 22(12), pp.799–805.

Allafta , J.A., Knight, R., Zebker, H. A., Schreuder, W. A., Agram, P. S. and Lauknes, T. R (2021): High quality InSAR data linked to seasonal change in hydraulic head for an agricultural area in the San Luis Valley, Colorado. Water Resources Research 47: 11.

Baba, A.; Tyfur, G. (2011): 'Groundwater Contamination and its Effect on Health in Turkey. Environ. Monit. Assess. 2011, 183, 77–94. [CrossRef] [PubMed]

Baishali Niyogi (2023); Assessment of Groundwater Depletion and its Socioeconomic Impacts in Arid Regions with special reference of Ahmedabad City International Journal of Research in Engineering and Science (IJRES) ISSN (Online): 2320-9364, ISSN (Print): 2320-9356 www.ijres.org Volume 11 Issue 11 ǁ November 2023 ǁ PP. 167-173

Doke H, (2018): Estimating the potential for expanding smallholder irrigation in Sub-Saharan Africa. Agicultural Water Management, 131, pp.183–193.

Galloway; J. Cunningham W. (2003): Ground-Water Depletion across the Nation U.S Geological Survey Fact Sheet 103-03 November 2003.

Girish, P.,Riccard, P., Cantone, A., Defilippi, M., Ogushi, F., and Galliano, S. (2011): Quantitative comparison of methods and sensors for monitoring land subsidence phenomena based on satellite SAR interferometric stacking. In Proceedings of the Geological Remote Sensing Group Annual Meeting 2011, December 7–9. Frascati, Italy: ESA ESRIN.

Hannes, L.; Cenci, L.; Tettamanti, M.; Berati, M. (2014): "Evaluating the environmental impact of various dietary patterns combined with different food production systems". European Journal of Clinical Nutrition. 61 (2): 279–286. doi:10.1038/sj.ejcn.1602522. PMID 17035955.

Hazell Greenburg (1992): The Ocean Moon: Search for an Alien Biosphere. Springer Praxis Books.

Kaewdum and Chotpantarat (2021). Impact of Changes in Groundwater Extractions and Climate Change on Groundwater-Dependent Ecosystems in a Complex Hydrogeological Setting. Water Resour. Manag. 2021, 32, 259–272. [Google Scholar] [CrossRef]

Kollert, W. C. (1969): Geology 2nd Edition Oxford University Press.

Dan Hassan S., K. Tiampo, P.J. Gonzalez, V. Manville, and G. Jolly. (2019): Ground deformation occurring in the city of Auckland, New Zealand, and observed by Envisat interferometric synthetic aperture radar during 2003-2007. Journal of Geophysical Research, Solid Earth 115: 12.

Mustapha, J., Bethune, J., Anderson, K. J., Syed, T. H., Swenson, S. C., deLinage, C. R., and Rodell, M. (2014): Satellites measure recent rates of groundwater depletion in California's Central Valley, Geophys. Res. Lett., 38, L03403, doi: https://doi.org/10.1029/2010GL046442 Wiley Online Library ADS Web of Science®Google Scholar

Mosuro P., (2012): Smallholder groundwater irrigation in Sub-Saharan Africa: country-level estimates of development potential Water International, 38(4), pp.392–407.

Nwankwo S. (2013). Pillar of Sand: Can the Irrigation Miracle Last? Norton, New York.

Rinkesh, A., B.F. Thomas, M.-H. Lo, J.T. Reager, J.S. Famiglietti, K. Voss, S. Swenson, and M. Rodell. (2018): 'Quantifying renewable groundwater stress with GRACE. Water Resources Research 51, no. 7: 5217–5238.

Winston (2009): 'Population Division of the Department of Economic and Social Affairs of the United Nations Secretariat. World Population Prospects: the 2006 revision and World Urbanization Prospects: the 2005 revision. http://esa.un.org.unpp.

Yeh, T.T., and T.J. Burbey. (2016): 'The value of subsidence data in ground water model calibration. Groundwater 46, no. 4: 538–550.

Kumari and Singh S., LoaIciga, H. A., Wolf, J. T. (2021). "Environmental impacts of groundwater overdraft: selected case studies in the south western United States". Environmental Geology. 47 (3): 396–404. doi: https://doi.org/10.1007/s00254-004-1164-3

Zolekar, M., T.J. Burbey, V.D.S. Nunes, and J. Borggaard (2018): 'A new zonation algorithm with parameter estimation using hydraulic head and subsidence observations. Groundwater 52: 514–524. DOI: https://doi.org/10.1111/gwat.12102